EUV Spectra of W^{13+} Ions in the Large Helical Device: Recent Progress in Observation of Tungsten Ions in Low to Intermediate Charge State Range for Fusion Plasma Diagnostics*)

Tetsutarou OISHI[1)], Ryota NISHIMURA[1)], Izumi MURAKAMI[2,3)], Daiji KATO[2,4)], Hiroyuki A. SAKAUE[2)], Motoshi GOTO[2,3)], Yasuko KAWAMOTO[2,3)], Tomoko KAWATE[2,3)], Nobuyuki NAKAMURA[5)], Hiroyuki TAKAHASHI[1)] and Kenji TOBITA[1)]

[1)]*Department of Quantum Science and Energy Engineering, Tohoku University, 6-6-01-2 Aobayama, Sendai 980-8579, Japan*

[2)]*National Institute for Fusion Science, National Institutes of Natural Sciences, 322-6 Oroshi-cho, Toki 509-5292, Japan*

[3)]*Graduate Institute for Advanced Studies, SOKENDAI, 322-6 Oroshi-cho, Toki 509-5292, Japan*

[4)]*Interdisciplinary Graduate School of Engineering and Sciences, Kyushu University, Kasuga 816-8580, Japan*

[5)]*Institute for Laser Science, The University of Electro-Communications, 1-5-1 Chofugaoka, Chofu 182-8585, Japan*

(Received 31 July 2024 / Accepted 10 October 2024)

Spectroscopic studies of emissions released from tungsten ions combined with a pellet injection technique have been conducted in the Large Helical Device for contribution to the tungsten transport study in tungsten divertor fusion devices and for expansion of the experimental database of tungsten line emissions. Emission lines were explored for the observation of low to intermediate charge states in the range of W^{10+} to W^{20+}, and the line spectra of W^{13+} were observed for the first time in fusion plasma experiments. The wavelengths of the observed W^{13+} lines were 243.1 Å, 247.6 Å, 248.3 Å, and 249.1 Å in the extreme ultraviolet wavelength range, and all of them were emission from the $4f^{13}5s^2$ - $4f^{13}5s5p$ transitions.

Keywords: plasma spectroscopy, extreme ultraviolet, magnetically confined fusion, impurity transport, tungsten ions in low charge states

DOI: 10.1585/pfr.20.2402009

1. Introduction

Plasma-facing components in nuclear fusion devices require a high melting point and low sputtering rate, thus tungsten (W) is the most promising candidate material. However, there is a concern that tungsten ions with a large atomic number of $Z = 74$ will cause large energy loss by radiation and ionization when the plasma is contaminated by the tungsten impurity. For contribution to the tungsten impurity transport study in fusion plasmas and for expansion of the experimental database of tungsten line emissions, spectroscopic studies for emissions released from tungsten ions have been conducted in the Large Helical Device (LHD), which is a superconducting plasma confinement device with a heliotron magnetic configuration [1]. The LHD spectroscopy system, which simultaneously measures the wavelength range from visible light to X-rays, enables simultaneous observation of tungsten ions from low to high charge states, resulting in successful observation of neutral particles of W^0 to highly charged ions of W^{46+} [2–5]. However, the observation of ions with low to intermediate charge states in the range of W^{10+} to W^{20+}, which are important for the study of tungsten transport in the edge plasma, is not sufficient, thus exploring useful emission lines for spectroscopic measurements in these charge states has remained one of the main concerns.

In order to explore the emission lines of unobserved charge states, it is useful to refer to the spectra observed in the Compact Electron Beam Ion Trap (CoBIT) experiments, and an example of a charge state that has actually been observed is W^{13+} [6]. The electronic ground state of W^{13+} is $1s^22s^22p^63s^23p^63d^{10}4s^24p^64d^{10}4f^{13}5s^2$, and some $4f^{13}5s^2$ - $4f^{13}5s5p$ transitions have been observed in the 240 - 250 Å of the extreme ultraviolet (EUV) wavelength region [7, 8]. In this study, we investigate whether

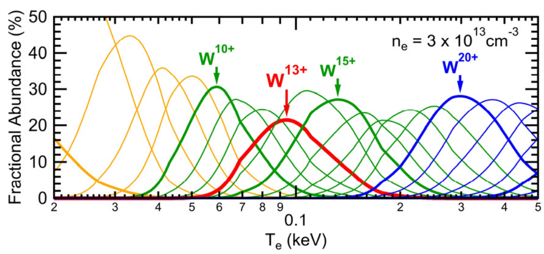

Fig. 1 Fractional abundance of tungsten ions in the electron temperature range of 0.02 keV to 0.5 keV.

author's e-mail: tetsutarou.oishi.a4@tohoku.ac.jp

*) This article is based on the presentation at the 26th International Conference on Spectral Line Shapes (ICSLS2024).

such W^{13+} emission lines can be also observed in the LHD plasmas. Figure 1 shows the electron temperature dependence of the fractional abundance ratios of tungsten ions including the W^{10+} to W^{20+} charge states, calculated using the ionization rate coefficients (data type 'ADF11', data file 'scd50_w.dat') and the recombination rate coefficients (data type 'ADF11', data file 'acd50_w.dat') available in the ADAS database [9]. The electron density of 3×10^{13} cm^{-3} was used in this calculation. W^{13+} ions have a maximum value when the electron temperature is around 100 eV. Therefore, in this study, we search for emission lines especially focusing on the spectra when the central electron temperature of the LHD plasma is less than 1 keV.

2. Tungsten Pellet Injection Experiment in LHD

For the spectroscopic measurement of tungsten ions at LHD, an "impurity pellet" consisting of a small piece of tungsten metal wire surrounded by carbon or polyethylene in the shape of a cylindrical tube is injected into the plasma [10]. Figure 2 shows a typical waveform of W pellet injection experiment in a hydrogen discharge with the position of the magnetic axis at 3.6 m and the toroidal magnetic field of 2.75 T in the clockwise direction. The plasma was initiatd by the electron cyclotron heating (ECH) and further heated by the neutral beam injection (NBI). Figure 2 (a) shows the injection power of ECH and NBI. The negative-ion source based NBI (n-NBI) contributed to the electron heating in the early half of the discharge, while the positive-ion source based NBI (p-NBI) contributed to the ion heating in the latter half of the discharge. The tungsten pellet was injected at t = 4.1 s, and the plasma response to this was observed as (b) a decrease in the central electron temperature, T_{e0}, and an increase in the line-averaged electron density, $\bar{n}_e$, and (c) a decrease in the plasma stored energy, W_p, and an increase in the total radiation power, P_{rad}. T_{e0} began to decrease from about 3.0 keV after pellet injection and remained close to zero during t = 5.3 - 5.9 s after switching the heating method from n-NBI to p-NBI.

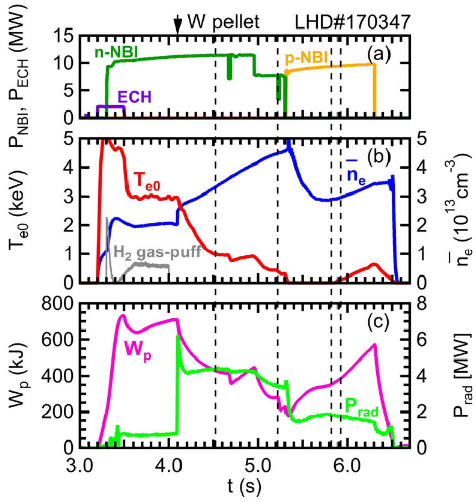

Fig. 2 Typical waveform of W pellet injection experiment in LHD: (a) heating power of ECH, n-NBI, and p-NBI, (b) central electron temperature, T_{e0}, and line-averaged electron density, $\bar{n}_e$, and (c) plasma stored energy, W_p and total radiation power, P_{rad}. Four vertical dashed lines indicate the four timings used in Fig. 3 for spectra analysis.

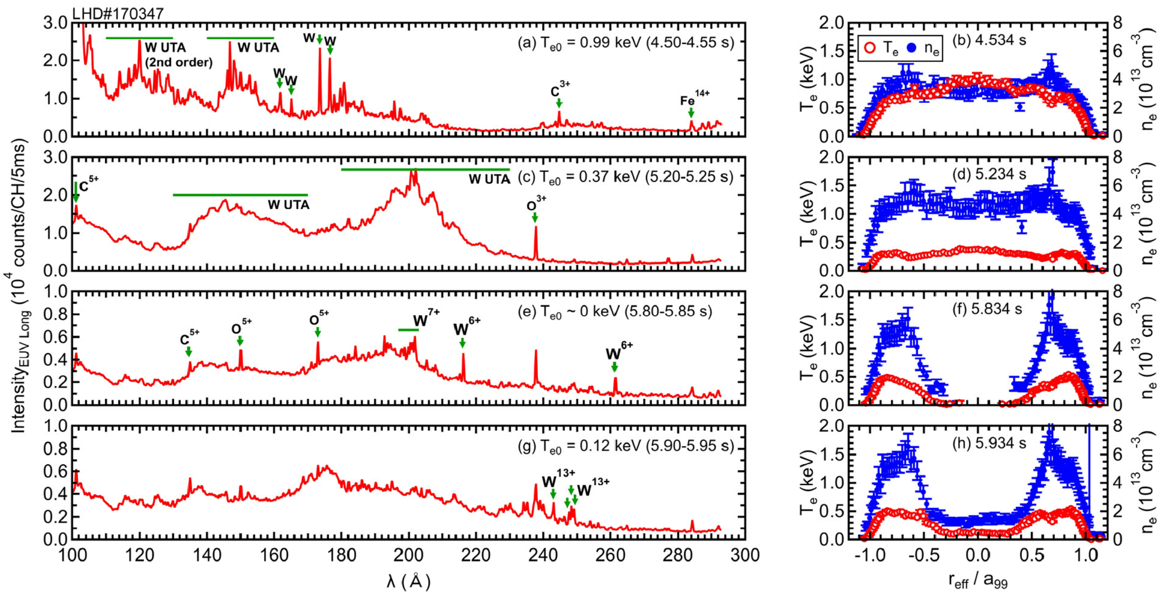

Fig. 3 EUV spectra including tungsten emission lines, and spatial profiles of electron temperature and electron density for the discharge shown in Fig. 2. The spectra and the profiles were measured at 4.50 - 4.55 s for (a, b), 5.20 - 5.25 s for (c, d), 5.80 - 5.85 s for (e, f), and 5.90 - 5.95 s for (g, h), respectively, and the spectral shape changed in response to changes in the electron temperature. In the T_e and n_e profiles, the locations of r_{eff} / a99 = ±1 are the plasma edges.

Thereafter, T_{e0} recovered to about 0.6 keV toward the termination of the discharge. In order to focus on tungsten ions with low charge states, the spectra after t = 4.5 s, in which T_{e0} falls below 1.0 keV, were carefully examined. Four vertical dashed lines in Fig. 2 indicate the four timings to be used in Fig. 3 for spectra analysis in the next chapter.

3. EUV Spectra of W^{13+} in the Wavelength Range of 240 - 250 Å

Figure 3 shows EUV spectra including tungsten emission lines, and spatial profiles of electron temperature, T_e, and electron density, n_e, for the discharge shown in Fig. 2. In this paper, spectra at wavelengths from 100 - 300 Å measured by a flat-field EUV spectrometer called "EUV Long" are presented [11]. The field of view of the EUV Long spectrometer covers the cross-section of the plasma almost from top edge to bottom edge, and has no spatial resolution. A CCD detector (1024 x 256 pixels, pixel size 26 x 26 μm^2, Andor DO420-BN) is located at the position of the exit slit of the spectrometer. The time resolution of the EUV spectroscopy is 5 ms, but the spectra shown in this paper were averaged over 10 data acquisitions to increase the signal-to-noise ratio, namely, they were averaged over 50 ms. The T_e and n_e profiles were measured using a Thomson scattering system [12]. T_e and n_e are plotted against the normalized minor radius, r_{eff} / a_{99}, where r_{eff} is the effective minor radius and a_{99} is the plasma edge, defined as the effective minor radius in which 99% of electron stored energy was enclosed. The spectra in Fig. 3 (a) were averaged over t = 4.50 - 4.55 s, and the T_{e0} obtained from the T_e profile in Fig. 3 (b) was 0.99 keV. Quasi-continuous spectra called Unresolved Transition Arrays (UTAs) were observed around 120 Å and 150 Å. Several discrete W lines were observed from 160 Å to 180 Å, but the charge states of these lines have not been identified yet. UTA was also observed in the spectrum Fig. 3 (c), where the T_{e0} evaluated from the T_e profile in Fig. 3 (d) was 0.37 keV. Identification of the charge state of the UTAs in this wavelength region has been attempted using calculations based on a combination of an atomic structure model and a collisional-radiative (CR) model [13]. Recent progress has shown that the UTA around 150 Å contains the charge regions of W^{21+} - W^{25+} [14] and 200 Å contains the charge regions of W^{17+} - W^{25+} [15, 16]. In the latter half of the discharge, the electron temperature dropped further, and a state in which T_{e0} took a value close to zero appeared. The spectrum at this time is shown in Fig. 3 (e), and as shown in Fig. 3 (f), both T_e and n_e have an extremely hollow spatial profiles called a "temperature hole" [17]. Associated with the low electron temperature, extremely low charge states such as W^{6+} and W^{7+} were observed. The electron temperature gradually recovered, and the spectrum at T_{e0} = 0.12 keV is shown in Fig. 3 (g). As shown in Fig. 3 (h), both T_e and n_e recovered to finite values at the center of the plasma. The four emission lines observed at 240 - 250 Å are W^{13+}. Identification of the charge states of these emission lines is possible by comparison with the spectra observed in the CoBIT experiment.

Figure 4 shows the EUV spectra of the wavelength region including the four W^{13+} emission lines, comparing the spectra observed at (a) LHD and (b) CoBIT at the University of Electro-Communications [18], and the spectrum calculated by the flexible atomic code (FAC), which is an atomic structure calculation code including CR model [19]. In the FAC calculation, the electron configurations of $4f^{14}nl$, $4f^{13}5snl$, $4f^{13}5p^2$, $4f^{13}5p5d$, $4f^{12}5s^25l$, and $4d^94f^{14}5s^2$ (n = 5 and 6, l = 0 – 4) were taken into account. The four emission lines observed at LHD are in good agreement with those already identified as W^{13+} in CoBIT. All of these emission lines are caused by $4f^{13}5s^2$ - $4f^{13}5s5p$ transitions, as reported in a previous study comparing a CoBIT experiment and a CR model calculation [7]. On the other hand, as shown in Fig. 4 (c), the calculated values of the wavelengths of the $4f^{13}5s^2$ - $4f^{13}5s5p$ emission lines by the FAC code were a few Å shorter than those obtained in the LHD and CoBIT experiments. This shift to shorter wavelengths has also been confirmed in calculations using other codes such as the HULLAC code [7] and the COWAN code [20]. Therefore, it is not considered to be a problem to identify the correspondence between the experimental and calculated emission lines. The main reason for the wavelength shift between experiments and calculations is considered to be the accuracy of the energy level calculations. Especially for high-Z ions in low charge states, which have a large number of electrons, the number of energy levels becomes enormous, and the way of considering their interactions can also affect the re-

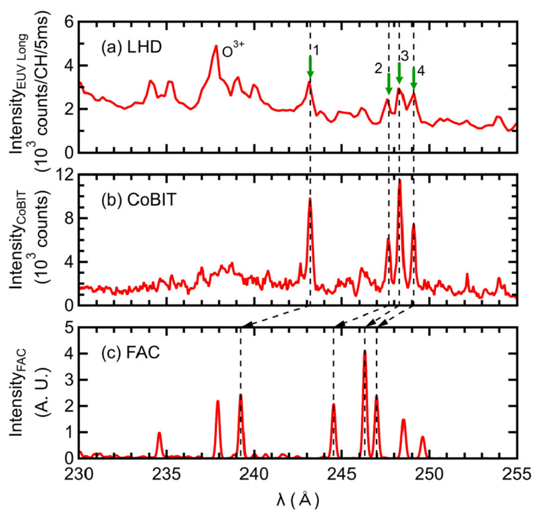

Fig. 4 EUV spectra including four W^{13+} emission lines from $4f^{13}5s^2$ - $4f^{13}5s5p$ transitions. (a) and (b) were measured at LHD and CoBIT, respectively, and (c) was calculated using the FAC code.

Table 1 Wavelengths of the four W^{13+} emission lines from the $4f^{13}5s^2$ - $4f^{13}5s5p$ transitions, numbered 1 - 4 in Fig. 4. J_{lower} and J_{upper} are the total angular momentum of the lower and upper levels, respectively. For the wavelength values, λ_{LHD} and λ_{CoBIT} were measured at LHD and CoBIT, respectively, and λ_{FAC} was calculated using the FAC code.

No.	J_{lower}	J_{upper}	λ_{LHD} (Å)	λ_{CoBIT} (Å)	λ_{FAC} (Å)
1	7/2	7/2	243.13 ± 0.05	243.181 ± 0.004	239.25
2	5/2	7/2	247.58 ± 0.04	247.663 ± 0.005	244.54
3	7/2	9/2	248.32 ± 0.08	248.324 ± 0.006	246.31
4	7/2	5/2	249.06 ± 0.08	249.086 ± 0.007	246.99

sults. In fact, even a comparison between calculations with the same FAC code as in this study and tungsten spectral measurements in high-temperature plasma experiments reported good agreement in wavelengths for the more highly charged W^{45+} and W^{46+} [21], or W^{47+} to W^{63+} [22]. Another interesting point about the spectrum in Fig. 4 (a) is that isolated emission lines with peaks at approximately 234 Å, 235 Å, 239 Å, and 240 Å are observed around the O^{3+} peak. The spectral shape is quite similar to that of W^{14+} observed in a CoBIT experiment [7], and if W^{14+}, this also means further exploration of the charge state region in the observation of tungsten emission lines in fusion plasma experiments. Detailed comparison among these emission lines with CoBIT experiments and FAC calculations will be performed in the future to identify the charge states.

Finally, Table 1 summarizes the wavelengths of the four W^{13+} emission lines observed at LHD and CoBIT and calculated by FAC, together with the total angular momentum of the lower and upper levels. This is the first time that W^{13+} emission lines have been identified in a fusion plasma experiment. In the observations of time evolution and spatial profiles of the emission intensity of tungsten ions up to W^{46+} that have recently progressed at LHD [23], spectroscopic data for tungsten ions with low charge states have been insufficient. Therefore, the W^{13+} emission lines observed in this study are expected to be a useful tool for monitoring the behavior of tungsten ions with low charge states.

4. Summary

Spectroscopic studies of emissions released from tungsten ions combined with a pellet injection technique have been conducted in LHD for contribution to the tungsten transport study in tungsten divertor fusion devices and for expansion of the experimental database of tungsten line emissions. Emission lines were explored for the observation of low to intermediate charge states in the range of W^{10+} to W^{20+}, and the line spectra of W^{13+} were observed for the first time in fusion plasma experiments. The wavelengths of the W^{13+} lines observed at LHD were 243.1 Å, 247.6 Å, 248.3 Å, and 249.1 Å in the EUV wavelength range, and through comparison with a CoBIT experiment and a calculation with the FAC code, all of them were confirmed to be emissions from the $4f^{13}5s^2$ - $4f^{13}5s5p$ transitions.

Acknowledgments

The authors thank all the members of the LHD team for their cooperation with the LHD operation. This work was partially supported by JSPS KAKENHI (Grant Numbers JP20K03896 and JP21H04460), the NIFS Collaboration Research program (Grant Numbers NIFS23KIPP031, NIFS23KIIP021, and NIFS23KIPF007). The data supporting the findings of this study are available in the LHD experiment data repository at https://doi.org/10.57451/lhd.analyzed-data.

[1] Y. Takeiri *et al.*, Nucl. Fusion **57**, 102023 (2017).
[2] S. Morita *et al.*, Springer Proceedings in Physics **271**, 23 (2022).
[3] T. Oishi *et al.*, Atoms **9**, 69 (2021).
[4] T. Oishi *et al.*, Phys. Scr. **96**, 025602 (2021).
[5] T. Oishi *et al.*, Phys. Scr. **91**, 025602 (2016).
[6] Priti *et al.*, Atoms **11**, 57 (2023).
[7] Y. Kobayashi *et al.*, Phys. Rev. A **92**, 022510 (2015).
[8] M. Mita *et al.*, J. Phys.: Conf. Ser. **875**, 012019 (2017).
[9] The ADAS Project, Version 2.1, 1995-2024. http://open.adas.ac.uk
[10] X.L. Huang *et al.*, Rev. Sci. Instrum. **85**, E811 (2014).
[11] M.B. Chowdhuri *et al.*, Rev. Sci. Instrum. **78**, 023501 (2007).
[12] K. Narihara *et al.*, Rev. Sci. Instrum. **72**, 1122 (2001).
[13] C. Suzuki *et al.*, J. Phys. B: At. Mol. Opt. Phys. **44**, 175004 (2011).
[14] I. Murakami *et al.*, 2nd IAEA Technical Meeting on the Collisional-Radiative Properties of Tungsten and Hydrogen in Edge Plasma of Fusion Devices, Vienna, Austria (2023).
[15] R. Nishimura *et al.*, Plasma Fusion Res. **19**, 1402022 (2024).
[16] R. Nishimura *et al.*, Nucl. Mater. Energy **41**, 101740 (2024).
[17] C. Suzuki *et al.*, Phys. Scr. **89**, 114009 (2014).
[18] N. Nakamura *et al.*, Rev. Sci. Instrum. **79**, 063104 (2008).
[19] M.F. Gu, Astrophys. J. **582**, 1241 (2003).
[20] U.I. Safronova *et al.*, Phys. Rev. A **88**, 032512 (2013).
[21] Ł. Syrocki *et al.*, J. Fusion Energy **39**, 194 (2020).
[22] J. Yanagibayashi *et al.*, J. Phys. B: At. Mol. Opt. Phys. **43**, 144013 (2010).
[23] T. Oishi *et al.*, Nucl. Fusion **64**, 106011 (2024).